Phase Noise Compensation for Nonlinearity-Tolerant Digital Subcarrier Systems With High-Order QAM

Yankov, Metodi Plamenov; Barletta, L.; Zibar, Darko

Published in:
IEEE Photonics Journal

Link to article, DOI:
10.1109/JPHOT.2017.2740983

Publication date:
2017

Document Version
Publisher's PDF, also known as Version of record

Phase Noise Compensation for Nonlinearity-tolerant Digital Sub-carrier Systems with High-order QAM

M. P. Yankov, *Member, IEEE*, L. Barletta, *Member, IEEE*, D. Zibar, *Member, IEEE*

Department of Photonics Engineering, Technical University of Denmark, 2800 Kgs. Lyngby, Denmark and Department of Electronics Information and Bioengineering, Politecnico di Milano, 20133 Milan, Italy

DOI: 10.1109/JPHOT.2009.XXXXXXX

This research was sponsored by the Danish National Research Foundation (DNRF) Research Centre of Excellence, SPOC, ref. DNRF123. This paper was presented in part at the European Conference on Optical Communications (ECOC), 2017.

Abstract: The fundamental penalty of sub-carrier modulation (SCM) with independent sub-carrier phase noise processing is estimated. It is shown that the fundamental signal-to-noise ratio (SNR) penalty related to poorer phase noise tolerance of decreased baudrate subcarriers increases significantly with modulation format size and can potentially exceed the gains of the nonlinear tolerance of SCM. A low complexity algorithm is proposed for joint sub-carrier phase noise processing, which is scalable in the number of sub-carriers and recovers almost entirely the fundamental SNR penalty with respect to single carrier systems operating at the same net data-rate. The proposed algorithm enables high-order modulation formats with high count of sub-carriers to be safely employed for nonlinearity mitigation in optical communication systems.

Index Terms: Multi-carrier, joint processing, phase noise, subcarrier multiplexing, WDM.

1. Introduction

Digital sub-carrier modulation (SCM) has recently attracted significant attention due to its resilience to nonlinearities in wavelength division multiplexed (WDM) optical fiber systems. Split-step simulations [1], [2], as well as theoretical predictions with the enhanced Gaussian noise model [3], [4], show that the symbol rate per channel can be optimized for maximum transmission reach to between 2 GBd and 10 GBd, also confirmed experimentally [5], [6]. A reach increase of between 5% and 25% is reported, depending on the scenario, with larger increase for QPSK than the 16-quadrature amplitude modulation (QAM) format. Recently, it was suggested that the gains may be significant also for higher-order modulation formats, e.g. 64QAM and 256QAM assuming nonlinear phase noise (NLPN) compensation is performed [7]. Around 9% gains were experimentally reported in [8] for 16QAM, where the impact of NLPN is also studied by employing a data-aided carrier phase recovery method. It was suggested that SCM systems with high-order modulation can significantly benefit from a more sophisticated phase noise compensation techniques, which allow for NLPN compensation. Similar conclusion is given in [9] for simulations of Gaussian modulation without laser phase noise, which simplifies the analysis and phase noise compensation.

The benefits of transmission of super-channels with several sub-carriers of optimized bandwidth

were also demonstrated in different context, e.g. with constellation shaping [10], as a function of the WDM bandwidth efficiency [11] or number of WDM channels [12].

The standard receiver architecture for multi-carrier (MC) systems performs independent processing of each sub-carrier. While the impact of I/Q skew and imbalance for such systems is studied and compensated by complex joint processing in e.g. [6], [13], the local oscillator phase noise is still processed independently with the simple Viterbi & Viterbi algorithm in [6], which is known to be sufficient for QPSK signals. However, for larger modulation formats, more sophisticated methods are needed to study the nonlinear tolerance of SCM. Alternatively, data-aided approaches are required as in e.g. [8], [10]. Carrier phase recovery is particularly problematic for MC systems, where the symbol rate per sub-carrier is smaller and each sub-carrier is thus more affected by local oscillator phase noise. The impact of joint carrier phase recovery with a modified Viterbi & Viterbi algorithm was studied for QPSK modulation [14], where the phase noise tolerance is significantly improved. Joint carrier phase recovery was proposed in [15] for 16QAM modulation. Higher order modulation are covered with the pilot-aided algorithm [16], later extended for multi-carrier processing [17]. Recently, an algorithm was proposed for joint sub-carrier phase noise compensation [18], which allows for SCM nonlinear gains to be achieved with up to 256QAM.

In this paper, the work from [18] is extended in the following manner. The impact of independent sub-carrier phase noise processing is studied in terms of lower and upper bounds on the capacity of standard, linear, phase noise channels (i.e. linear transmission). The lower bound on the capacity of a single carrier system with transmitter and receiver lasers with a linewidth (LW) of up to 1 MHz is compared to the upper bound on the capacity of SCM with the same lasers. Having fixed an information rate target, these capacity bounds give signal-to-noise ratios (SNRs) whose difference is reported as a penalty. Under the fair assumption that the laser phase noise and the nonlinear noise in fibers are independent and uncorrelated processes, the penalty will be present in the nonlinear transmission regime and is also independent of the nonlinear gains offered by SCM in such scenarios. The penalty is therefore *fundamental*. The complete mathematical derivation is then provided for the algorithm proposed in [18], and it is demonstrated that the fundamental penalty of SCM can be recovered almost entirely at no additional complexity when all sub-carriers are processed jointly. Finally, nonlinear gains are demonstrated with the proposed algorithm for up to 256QAM.

2. Channel model

A linear phase noise channel is considered, where the local oscillator (LO) and transmitter laser are modeled as Wiener processes. The channel is of the form

$$y_t = x_t \cdot e^{j\phi_t} + n_t, \tag{1}$$

where y_t and x_t are the channel output and input, respectively, n_t are additive, white Gaussian noise (AWGN) samples, ϕ_t are the phase noise samples at times $t \cdot T_s$, T_s is the sampling period and $t \in \mathbb{Z}$. The samples ϕ_t model the combined effect of transmitter laser and LO, and evolve as

$$\phi_t = \phi_{t-1} + v_t, \tag{2}$$

where v_t are samples from a zero-mean Gaussian process with variance $\gamma^2_{T_s} = 2 \cdot 2\pi\Delta_f T_s$. The laser linewdith Δ_f is assumed equal at transmitter and receiver for simplicity.

A block diagram of the considered system is given in Fig. 1. At the transmitter, multiple sub-carriers are combined into a digital super-channel by up-sampling and pulse shaping. The samples x_k in each sub-carrier at time $k \cdot T$ come from a finite-size constellation $\mathcal{X}$, in this paper QAM. The digital super-channel symbol period is $T = m \cdot N_{sc} \cdot T_s$, where m is the oversampling factor and N_{sc} is the number of sub-carriers. At the receiver, the sub-carriers are down-converted, down-sampled to 1 sample per symbol and sent for processing. Under the assumption that the inter-sub-carrier interference is negligible (see Section 5 for justification), the equivalent channel

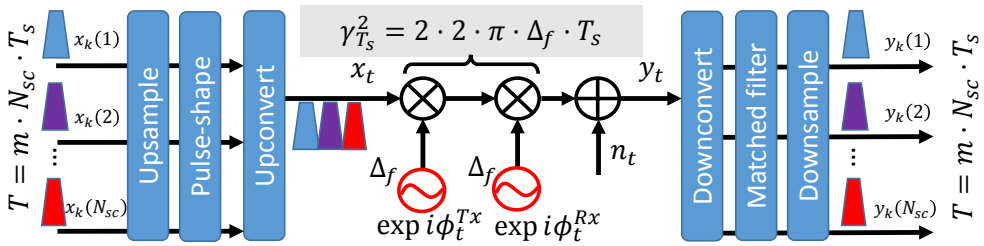

Fig. 1. A block diagram of the model for the considered system. Independent data modulate each sub-carrier. The sub-carriers are digitally combined and sent on the channel. At the receiver, down-conversion, matched filtering and down-sampling to 1 sample per symbol is performed in each sub-carrier.

for N_{sc}^{JP} jointly processed sub-carriers can be modeled as a diagonal multiple-input multiple-output (MIMO) channel of the form

$$\begin{bmatrix} y_k(1) \\ y_k(2) \\ \vdots \\ y_k(N_{sc}^{JP}) \end{bmatrix} = \begin{bmatrix} x_k(1) \\ x_k(2) \\ \vdots \\ x_k(N_{sc}^{JP}) \end{bmatrix} \cdot e^{j\theta_k} + \begin{bmatrix} n_k(1) \\ n_k(2) \\ \vdots \\ n_k(N_{sc}^{JP}) \end{bmatrix}. \tag{3}$$

Similar to the process $\{\phi_t\}$, the phase noise $\{\theta_k\}$ is modeled as a Wiener process with process noise variance $\gamma_T^2 = 2 \cdot 2\pi\Delta_f T$.

3. Fundamental penalty of independent sub-carrier processing

The information rate transferred through the phase noise channel for a given constellation and laser linewidth Δ_f is given by the mutual information (MI) $\mathcal{I}(X;Y)$ between the channel input and output, and is not known in closed form. The MI is measured in bits/symbol and provides an ultimate limit to the data rate, achievable by ideal forward error-correcting (FEC) code and ideal phase noise processing. When normalized by the occupied bandwidth and the symbol period, the MI provides the spectral efficiency of the system in bits/s/Hz. In SCM, even-though the phase noise originates at the same LO in all sub-channels, the independent phase processing results in parallel channels with equivalent MI, dependent on the *per-sub-carrier* symbol period T. Using the methods in [19], tight upper and lower bounds on $\mathcal{I}(X;Y)$ can be obtained. In order to obtain a fair estimate, i.e. a lower bound on the SNR penalty associated with SCM and the increased effective γ^2, the *upper bound* on the MI of an SCM system can be compared to the *lower bound* on the MI of a single carrier system. The difference between these bounds provides a lower bound on the fundamental penalty of SCM. An example of such bounds is given in Fig. 2, where single carrier 56 GBd system is compared to SCM with $N_{sc} = 10$ and $N_{sc} = 25$ for a $\Delta_f = 100$ kHz lasers at transmitter and receiver. The number of jointly processed sub-carriers is $N_{sc}^{JP} = 1$. The MI is limited by the size of the constellation to $\mathcal{I}(X;Y) < \log_2(|\mathcal{X}|)$. An ideal 25% FEC can correct all transmission errors if $\mathcal{I}(X;Y) > \frac{4}{5}\log_2(|\mathcal{X}|)$. The required SNR to achieve this MI is taken as a benchmark in this paper, and the difference in the required SNR is reported as penalty. As seen in Fig. 2, the fundamental penalty with 100 kHz lasers for 16QAM can be estimated to ≈ 0.2 dB, which is increased to around 0.6 dB for 256QAM when 25 sub-carriers are used, 2.24 GBd each.

A summary of the penalty at the above mentioned 25% FEC threshold for different laser linewidths is given in Fig. 3. The penalty lower bound of $N_{sc} = 1$ appears negative since the MI upper bound is always above the lower bound. In addition to the above mentioned lower bound on the penalty, and upper bound on the penalty can be estimated as the difference between the upper bound of the single carrier and the lower bound of SCM performance. The fundamental penalty upper bound is given with dashed lines in Fig. 3. The true fundamental penalty is confined

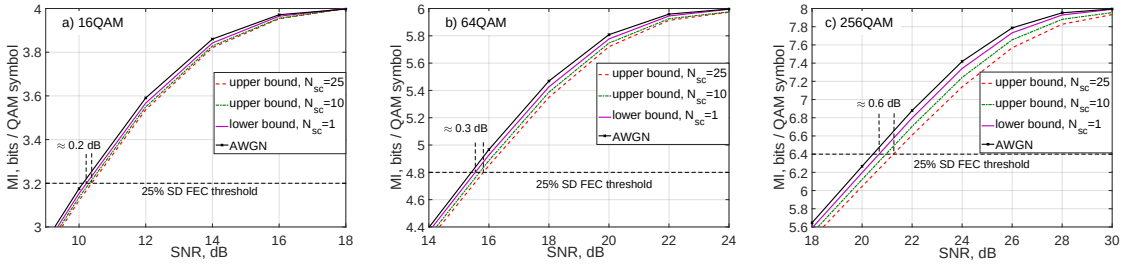

Fig. 2. MI bounds for SCM with laser linewidths 100 kHz. **a)** 16-,**b)** 64- and **c)** 256-QAM. The fundamental penalty is reported as the difference in the required SNR for achieving the 25% FEC error-free performance between the lower bound of single carrier system and the upper bound of SCM.

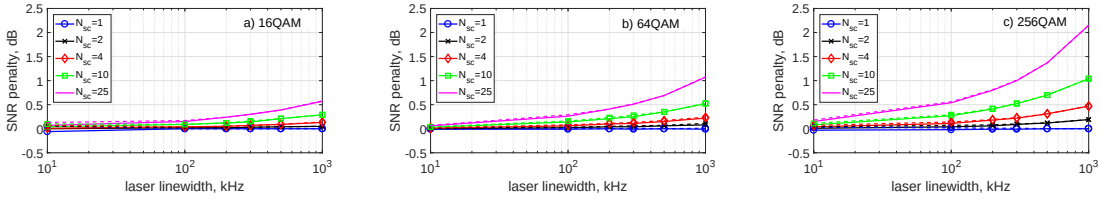

Fig. 3. Upper (**dashed lines**) and lower (**solid lines**) bounds on the fundamental penalties for different laser linewidths. The penalty is measured as the difference in the required SNR to achieve the 25% FEC overhead threshold.

between its upper and lower bounds, with a gap of < 0.05 dB in all cases. When the modulation format size is increased, the fundamental penalty is also increased, especially for poorer lasers. For 256QAM, the penalty can exceed 1 dB in some cases of interest.

4. Low-complexity joint sub-carrier processing

While the fundamental penalty is estimated from theoretical upper and lower bounds on the MI, practical transceivers operate at a lower rate compared to the theoretical limits. A more proper comparison between SCM and single carrier systems is thus achieved by comparing their achievable information rates (AIRs), which are lower bounds to the capacity of the phase noise channel. Previously, a low-complexity method was proposed for phase noise processing [20], which is able to operate at a low SNR relative to the modulation format size, e.g. at the 25% FEC limit. The method, referred to as the Tikhonov Mixture Model (TMM), was shown to outperform standard decision-directed methods, which are penalized due to the increased symbol error rate at that operating point where the uncoded BER is $\approx 10^{-1}$. The performance of the algorithm in [20] is given in Fig. 4 for 256QAM with 100 kHz lasers for different N_{sc} and $N_{sc}^{JP} = 1$. The penalty of the algorithm is ≈ 1.2 dB w.r.t. the capacity lower bound from Fig. 2. The penalty is then increased by another ≈ 4.3 dB for $N_{sc} = 13$.

The proposed extension to the TMM algorithm is given below. The set of jointly processed sub-carriers is denoted as $X_{N_{sc}^{JP}} = \{X(1), X(2), \dots X(N_{sc}^{JP})\}$ ($Y_{N_{sc}^{JP}} = \{Y(1), Y(2), \dots Y(N_{sc}^{JP})\}$, respectively), and the realization of the symbols on those sub-carriers at time k is $\mathbf{x}_k$. The sequence from time 1 to K is $\mathbf{x}_1^K$. The AIR per sub-carrier is estimated from the MI as

$$\begin{aligned}\mathcal{I}(X;Y) &= \frac{1}{N_{sc}^{JP}}\left[\mathcal{H}(X_{N_{sc}^{JP}}) - \mathcal{H}(X_{N_{sc}^{JP}}|Y_{N_{sc}^{JP}})\right] \\ &= (1-P)\cdot\log_2|\mathcal{X}| + \frac{1}{N_{sc}^{JP}}\lim_{K\to\infty}\frac{1}{K}\log_2 p(\mathbf{x}_1^K|\mathbf{y}_1^K),\end{aligned} \tag{4}$$

where $\mathcal{H}$ is the entropy operator and P is the pilot rate, which limits the maximum achievable

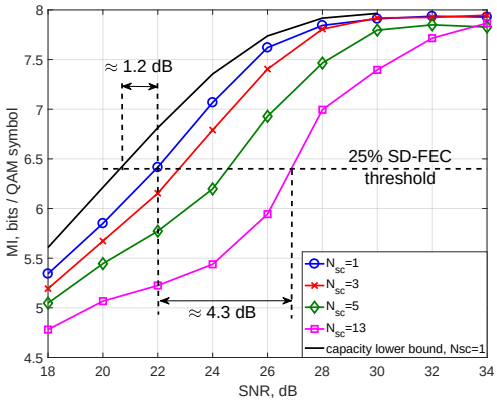

Fig. 4. Performance of the TMM algorithm, 256QAM with 100 kHz linewidth transmitter and receiver lasers. The algorithm uses 0.5% pilots, which are taken into account in the MI estimation. The sub-carriers are processed independently. At the 25% FEC threshold, significant penalty is observed for SCM, substantially larger than the fundamental penalty.

AIR. In (4), uniform input probability mass function p_X is assumed for simplicity, however, it is generally not a requirement. As demonstrated in [21], the algorithm in [20] can be applied also for probabilistically shaped systems, for which p_X is optimized. Estimating the true posteriors $p(\mathbf{x}_1^K|\mathbf{y}_1^K)$ is generally intractable. Instead, the approximation $p(\mathbf{x}_1^K|\mathbf{y}_1^K) = \prod_k p(\mathbf{x}_k|\mathbf{y}_1^K)$ is adopted in this paper, leading to an upper bound on the entropy $\mathcal{H}(X_{N_{sc}^{JP}}|Y_{N_{sc}^{JP}})$ and thus a lower bound on the AIR [22].

The receiver's task is to estimate the posterior distributions of the transmitted symbols (also referred to as the posteriors for brevity) $p(\mathbf{x}_k|\mathbf{y}_1^K)$, which are used both for AIR estimation, but also for the sub-sequent demodulation. The TMM algorithm estimates these posteriors by forward and backward recursions on a factor graph, where the forward message $p(\theta_k|\mathbf{y}_1^{k-1})$ and backward message $p(\mathbf{y}_{k+1}^K|\theta_k)$ are modeled as mixtures of Tikhonov distributions of variable θ_k

$$p(\theta_k|\mathbf{y}_1^{k-1}) = \sum_{m=1}^{M} \bar{\alpha}_{m,k} t(\bar{w}_{m,k};\theta_k),$$
$$p(\mathbf{y}_{k+1}^K|\theta_k) = \sum_{n=1}^{N} \bar{\beta}_{n,k} t(\bar{u}_{n,k};\theta_k). \tag{5}$$

In (5), $\bar{\alpha}_{m,k}$ and $\bar{\beta}_{n,k}$ are mixing coefficients, $t(w;\theta_k)$ is the Tikhonov distribution of variable θ_k with complex parameter w, and M and N are the number of mixture components in the forward and backward recursions, respectively. Joint sub-carrier processing requires replacing the scalar math in the recursions by vector math. The graph messages remain Tikhonov mixtures in θ_k, however, the mixture distribution parameters $\bar{w}_{m,k}$ and $\bar{u}_{n,k}$ can be estimated more accurately, leading to an improved performance. The complete derivations of (5) updated from the formulae in [20] to vector math are given in the Appendix. The final posteriors can be expressed as

$$p(\mathbf{x}_k|\mathbf{y}_1^K) = p(\mathbf{x}_k) \sum_{m=1}^{M} \bar{\alpha}_{m,k} \sum_{n=1}^{N} \bar{\beta}_{n,k} \int_{-\pi}^{\pi} p(\mathbf{y}_k|\mathbf{x}_k,\theta_k) t(\bar{u}_{n,k};\theta_k) t(\bar{w}_{m,k};\theta_k) d\theta_k. \tag{6}$$

Under the model (3), the likelihood in (6) factorizes as $p(\mathbf{y}_k|\mathbf{x}_k,\theta_k) = \prod_i p(y_k(i)|x_k(i),\theta_k)$, and assuming the data on different sub-carriers are independent, the posteriors can be expressed as

$$p(\mathbf{x}_k|\mathbf{y}_1^K) = \sum_{m=1}^{M} \bar{\alpha}_{m,k} \sum_{n=1}^{N} \bar{\beta}_{n,k} \prod_i p(x_k(i)) \int_{-\pi}^{\pi} p(y_k(i)|x_k(i),\theta_k) t(\bar{u}_{n,k};\theta_k) t(\bar{w}_{m,k};\theta_k) d\theta_k. \tag{7}$$

Using the methods in [20], the integrand in Eq. (7) is expressed as a product of three Tikhonov distributions of variable θ_k, and the integral is solved in closed form.

Mixtures of Tikhonov distributions were also proposed for phase noise tracking with constant amplitude constellations (e.g. PSK) input [23], which allows for simplified message estimation but cannot be used with e.g. QAM signals. Similar algorithm was proposed in [24] which is not constrained to PSK constellations, but employs a single Tikhonov distribution instead of a mixture for the messages and relies on iterative decoding to bootstrap the phase estimation, especially in strong phase noise scenarios. The algorithm proposed here and in [20] is derived for arbitrary alphabets and in the general case of multiple mixture components.

5. Results

5.1. Linear channel

The proposed algorithm is evaluated on the system of Fig. 1. The system parameters are given in Table I. It was verified in an ideal laser scenario that the 0.001 roll-off factor of the pulse-shaping filters with 50 MHz guardband does not result in measurable linear inter-sub-carrier interference. The number of mixture components in the Tikhonov recursions was optimized to $M = N = 4$, as no improvement was seen for larger values. The pilot symbols are used by replacing the prior probability in (7), (14) and (19) with $p(x_k(i)) = 1$ for the true transmitted symbol on the $i-$th sub-carrier at pilot symbol time $k \in \mathcal{K}_p(i)$, and with $p(x_k(i)) = 0$ for the rest of the symbols in the alphabet. For all other symbol positions, $p(x_k(i)) = 1/|\mathcal{X}|$. The pilot symbols are spread through the sub-carrier sequences as uniformly as possible as shown in Fig. 5, and the pilot positions $\mathcal{K}_p(i)$ on the $i-$th subcarrier are given by

$$\mathcal{K}_p(i) := \left\lfloor \frac{(i-1)}{i} \cdot \left(\frac{1}{P} - 1 \right) \right\rfloor + 1 + l \cdot \frac{1}{P}, \tag{8}$$

where $l \in \mathbb{N}_0, l \leq \lfloor K \cdot P \rfloor$. The pilot rate was optimized to ≈ 0.5 %. Higher pilot rate allows for improved phase noise estimation and tracking, however, it results in increased loss in maximum AIR, and ultimately worse performance. For comparison, in [16], 2% pilot rate is used for 256QAM, which is not taken into account in their penalty estimation. Furthermore, the target AIR and SNR in [16] are higher (as mentioned in Section 4), and the requirement to the phase noise tracking performance is thus not as strict[1].

In Fig. 6, the average AIRs are given for an $N_{sc} = 13$ system with the proposed modified TMM algorithm for a different number of jointly processed sub-carriers N_{sc}^{JP}. The laser linewidth is 100 kHz. When only 3 sub-carriers are jointly processed, the penalty is decreased by more than 2 dB at the FEC threshold. When all sub-carriers are jointly processed, the penalty of SCM w.r.t. single carrier system virtually vanishes. In Fig. 7, a summary of the penalty is given for 16QAM, 64QAM and 256QAM as a function of the laser linewidth. The penalty in this case is given w.r.t. the lower bound on the capacity of single carrier system. When $\Delta_f = 500$ kHz, SCM with independent sub-carrier processing did not achieve the FEC threshold. When the carriers are processed jointly, the penalty is decreased and for $N_{sc}^{JP} = N_{sc}$ the performance of a single carrier system is virtually achieved.

5.2. Fiber transmission

The proposed method is finally studied in a standard, single mode fiber transmission simulated with the split-step Fourier method (SSFM). Lumped amplification with erbium doped fiber amplifiers (EDFAs) is considered. For simplicity, single polarization WDM system is simulated, in which each WDM channel (also referred to as digital super-channel previously in the paper) consists of

[1]It is noted that the required SNR for the 25% FEC threshold is more than 3 dB lower than for BER$= 10^{-2}$. We have verified that at their target rate of BER$= 10^{-2}$, the TMM algorithm achieves similar performance in the single carrier case at similar values of $\Delta_f \cdot T_s$.

TABLE I
SYSTEM PARAMETERS FOR THE SIMULATION OF LINEAR CHANNELS

sub-carrier guardband	50 MHz
symbol rate per carrier	56 / N_{sc} GBd
total bandwidth	56 GHz + $(N_{sc}-1)\cdot 50$ MHz
laser LW range	10, 100, 200, 500 kHz
pulse shape filter	square root raised cosine
roll-off	0.001
oversampling factor m	4
pilot rate P	0.5 %
sequence length	10^5 symbols per sub-carrier
TMM mixture components M, N	$M = N = 4$

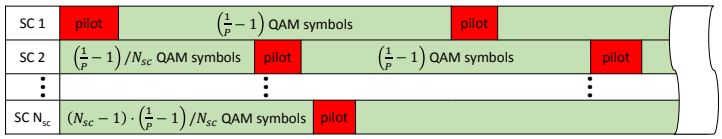

Fig. 5. Pilot spreading illustration.

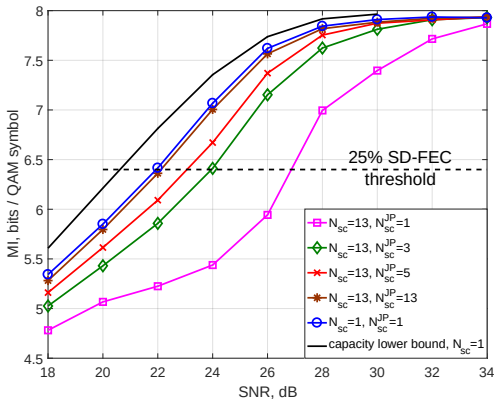

Fig. 6. AIR of the proposed updated TMM algorithm for 256QAM and 100 kHz laser linewidth. When all sub-carriers are processed jointly, there is virtually no penalty w.r.t. single carrier system.

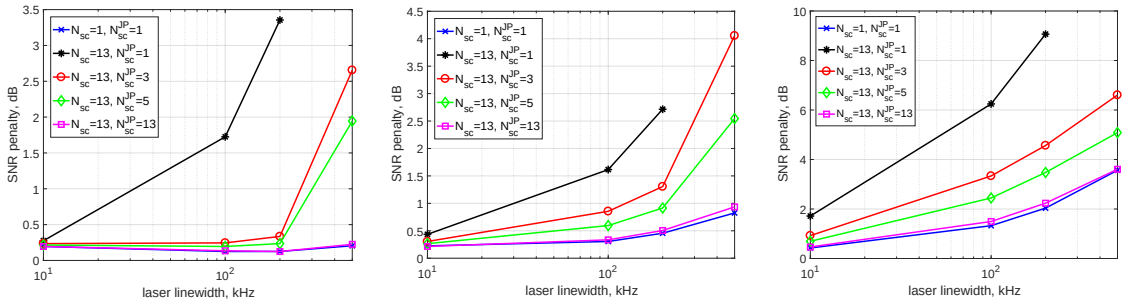

(a) 16QAM (b) 64QAM (c) 256QAM

Fig. 7. Penalties w.r.t. single carrier capacity lower bound. The penalty is almost completely recovered by jointly processing all sub-carriers.

N_{sc} sub-carriers. The central channel is evaluated. In the case where $N_{sc}^{JP} = N_{sc}$, the average performance of all subcarriers is reported. The transmission parameters are given in Table II.

In Fig. 8, the AIR is given as a function of the distance for 16, 64 and 256QAM at the optimal

TABLE II
FIBER TRANSMISSION PARAMETERS

no. of WDM channels	3
laser linewidth	0.01 and 100 kHz
subcarrier guardband	50 MHz
WDM channel guardband	500 MHz
WDM channel bandwidth	56 GHz + $(N_{sc}-1)\cdot 50$ MHz
no. of subcarriers N_{sc}	1, 5, 13
fiber loss	0.2 dB/km
nonlinear coefficient	$1.3\ (\mathrm{W}\cdot\mathrm{km})^{-1}$
dispersion	17 ps$/(\mathrm{nm}\cdot\mathrm{km})$
EDFA noise figure	5 dB
span length	100 km
SSFM step size	1 km

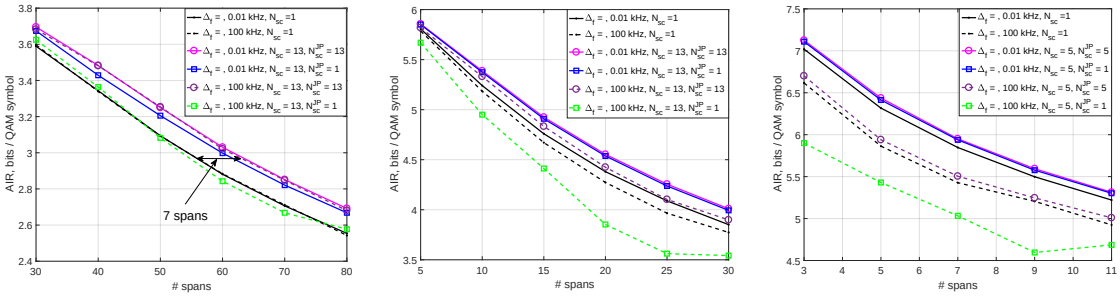

(a) 16QAM (b) 64QAM (c) 256QAM

Fig. 8. Performance for WDM transmission of SCM and single carrier systems. Nonlinear gain is achieved for all modulation formats - 10% for 256QAM and increased to 15% for 16QAM, independently of the laser linewidth. The proposed method achieves additional NLPN compensation gain.

total launch power (≈ 4 dBm and ≈ 5 dBm for single carrier and SCM systems, respectively). The number of sub-carriers was optimized to $N_{sc}=13$ at 50 spans and 20 spans for 16QAM and 64QAM, respectively, and to $N_{sc}=5$ at 5 spans for 256QAM. In the case of insignificant laser phase noise ($\Delta_f = 10$ Hz), for 16QAM, between 5 and 10 spans, corresponding to between 10% and 15% can be gained at short and long distance, respectively. This gain is purely due to the nonlinear tolerance of SCM, and is slightly increased when joint phase noise processing is performed. We attribute this additional gain to improved NLPN compensation, which was also previously demonstrated for the proposed algorithm [25], [26]. The additional gain for joint processing also suggests that the NLPN is correlated across sub-carriers, which is exploited with the proposed joint TMM algorithm. The gains are preserved when non-ideal lasers are employed ($\Delta_f = 100$ kHz), whereas for independent sub-carrier processing, the nonlinear tolerance gains of SCM are masked by the loss, originating in poorer laser phase noise compensation.

Joint phase noise processing enables around 2 spans of gain for 64QAM and less than a span for 256QAM regardless of the laser linewidth. The gains are generally smaller than the 16QAM gains from Fig. 8(a) due to the shorter distance and correspond to ≈ 10% of reach. Finally, in order to estimate the modulation format dependence of the SCM nonlinear tolerance, 256QAM was simulated at longer distances (lower AIR, respectively). In Fig. 9, the results are shown for 256QAM at distances similar to the 16QAM from Fig. 8(a). The number of sub-carriers is optimized to $N_{sc}=13$. At ≈5000 km distance, the gain is 5 spans (reduced to 4 spans with 100 kHz lasers), compared to the 7 spans (≈ 14%) gain with 16QAM at such distances. The gain is then increased to 7 spans at longer distances. SCM for high-order constellations can therefore still be of interest provided that the laser phase noise is properly compensated.

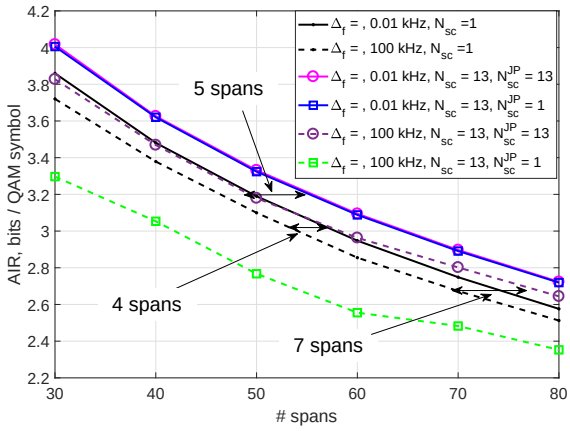

Fig. 9. AIR of SCM with 256QAM at long distances. Gains of 5 spans are achieved with pseudo-ideal lasers, which is reduced to 4 spans for lasers with 100 kHz linewidth at 5000 km, and increased to around 7 spans at longer distances.

6. Complexity

As discussed in [20], the basic TMM algorithm is simpler than standard decision-directed algorithms which rely on sliding window phase averaging. Estimating the posteriors in the joint TMM requires exactly the same amount of computations as independently processing each sub-carrier (see the factorization in Eq. (7)). The difference is only at the parameter update stages (Eq. (16) and Eq. (21)), which also requires the same computations as the standard algorithm applied to each sub-carrier independently. We conclude that there is no added complexity from the updated algorithm, which scales linearly with N_{sc}^{JP}.

The results above are obtained with $K = 10^5$ symbols. However, practical implementations require block-based processing and heavy parallelization. The algorithm processes all sub-carriers jointly and is thus naturally parallelized. The short block length performance of the algorithm with 256QAM, 100 kHz lasers and joint sub-carrier processing is studied in Fig. 10, where the SNR penalty of short block processing is reported w.r.t. the results in Fig. 6 at the 25% FEC threshold. In this case, overlap between blocks is allowed, which mitigates the effect of improper parameter estimation at block edges. A trade-off can be directly seen between the degree of overlap in the blocks, the block length and the pilot rate. High pilot rate allows for short blocks with small overlap, but result in a fixed penalty, related to the reduced maximum AIR. The block length can also be decreased if sufficient overlap is allowed between the blocks. The parameter optimization is thus a design choice.

7. Future work

As mentioned in Section 2, the diagonal MIMO channel (3) is valid under the assumption of insignificant inter-sub-carrier interference. This assumption becomes too strong for nonlinear fiber transmission due to cross-phase modulation and four-wave mixing. Both the inter-sub-carrier and intra-channel cross-talk effects would generally require a more complex model, akin to phase noise models for e.g. orthogonal frequency division multiplexed systems [27] or full-blown MIMO channels [28] for phase noise mitigation. Due to the non-linear nature of the cross-talk, the effectiveness of such models is unknown. Furthermore, digital chromatic dispersion compensation will induce dispersion enhanced phase noise as discussed in [15], which is neglected in this work. Adopting the proposed algorithm to such cases is an interesting area for future research.

As seen in Fig. 6, a slight performance degradation of SCM w.r.t. single carrier is still present. Whether the origin of this penalty is fundamental or simply due to algorithm sub-optimality is also

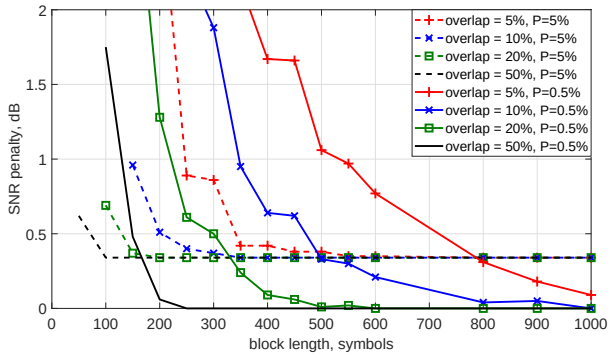

Fig. 10. Practical trade-offs for the proposed algorithm. Large overlap allows for reduced block length, even more so with increased pilot rate P.

an interesting problem left for future work.

8. Conclusion

The fundamental and practical penalties of sub-carrier modulation w.r.t. single carrier system operating at the same rate originating in reduced laser phase noise tolerance have been investigated. It was shown that joint sub-carrier processing is required in order to mitigate the fundamental penalty. An algorithm was proposed for joint sub-carrier processing operating at no additional complexity, which achieves the performance of single carrier system for wide range of laser linewidths. The proposed algorithm allows for digital sub-carrier modulation to be safely employed for non-linear noise mitigation in WDM systems operating with high-order QAM.

Appendix

The forward and backward recursions are defined as (Eq. (11) and Eq. (12) in [20])

$$p(\theta_k|\mathbf{y}_1^k) = \sum_{m=1}^{M} \alpha_{m,k} t(w_{m,k};\theta_k), \tag{9}$$

$$p(\mathbf{y}_k^K|\theta_k) = \sum_{n=1}^{N} \beta_{n,k} t(u_{n,k};\theta_k). \tag{10}$$

The update parameters for the backward message (5) can then be found as

$$\bar{\beta}_{n,k} = \beta_{n,k+1}, \qquad \bar{u}_{n,k} = \frac{u_{n,k+1}}{1+\gamma_T^2|u_{n,k+1}|}. \tag{11}$$

In order to complete the recursion, the updates for $\beta_{n,k}$ and $u_{n,k}$ are found from the following:

$$\begin{aligned} p(\mathbf{y}_k^K|\theta_k) &= p(\mathbf{y}_k|\theta_k,\mathbf{y}_{k+1}^K)p(\mathbf{y}_{k+1}^K|\theta_k) \\ &= \sum_{n=1}^{N} \bar{\beta}_{n,k} \sum_{\mathbf{x}_k\in\mathcal{X}^{N_{sc}^{JP}}} p(\mathbf{x}_k)p(\mathbf{y}_k|\mathbf{x}_k,\theta_k)t(\bar{u}_{n,k};\theta_k) \\ &\propto \sum_{n=1}^{N} \sum_{\mathbf{x}_k\in\mathcal{X}^{N_{sc}^{JP}}} \prod_i \mu_{n,k}(x_k(i))t(\bar{u}_{n,k}+2\cdot\mathsf{SNR}\cdot y_k(i)x_k(i)^*;\theta_k), \end{aligned} \tag{12}$$

where due to the model (3) the likelihood factorizes as $p(\mathbf{y}_k|\mathbf{x}_k,\theta_k)=\prod_i p(y_k(i)|x_k(i),\theta_k)$ and is expressed as a Tikhonov approximation to the Gaussian

$$p(\mathbf{y}_k|\mathbf{x}_k,\theta_k)\approx\prod_i\frac{2\cdot\mathsf{SNR}\cdot I_0(2\cdot\mathsf{SNR}|y_k(i)x_k(i)^*|)}{\exp(\mathsf{SNR}(|y_k(i)|^2+|x_k(i)|^2))}t(2\cdot\mathsf{SNR}\cdot y_k(i)x_k(i)^*;\theta_k). \tag{13}$$

In (12) we have used the fact that the product of two Tikhonov distributions may also be expressed as a Tikhonov distribution in order to calculate the sub-component mixture coefficient

$$\mu_{n,k}(x_k(i))=\frac{\bar{\beta}_{n,k}\cdot p(x_k(i))I_0(|\bar{u}_{n,k}+2\cdot\mathsf{SNR}\cdot y_k(i)x_k(i)^*|)}{I_0(|\bar{u}_{n,k}|)\exp(\mathsf{SNR}\cdot|x_k(i)|^2)}. \tag{14}$$

Due to the discrete nature of the input constellation, the number of components needed for tracking the phase noise grows exponentially with time. In order to avoid this problem, we propose an approximation to the inner sum in (12), where at each step we only take the sub-component with the largest mixing coefficient

$$\hat{x}_{n,k}(i)=\arg\max_{x_k(i)\in\mathcal{X}}\mu_{n,k}(x_k(i)), \tag{15}$$

$$u_{n,k}=\bar{u}_{n,k}+2\cdot\mathsf{SNR}\cdot\mathbf{y}_k\hat{\mathbf{x}}_{n,k}^H, \tag{16}$$

$$\beta_{n,k}=B\cdot\prod_i\mu_{n,k}(\hat{x}_{n,k}(i)), \tag{17}$$

where B is such that $\sum_{n=1}^N\beta_{n,k}=1$.

Similarly, the parameters for the predictive forward distribution appearing in (5) are found as

$$\bar{\alpha}_{m,k}=\alpha_{m,k-1},\qquad \bar{w}_{m,k}=\frac{w_{m,k-1}}{1+\gamma_T^2|w_{m,k-1}|}, \tag{18}$$

and

$$\rho_{m,k}(x_k(i))=\frac{\bar{\alpha}_{m,k}\cdot p(x_k(i))I_0(|\bar{w}_{m,k}+2\cdot\mathsf{SNR}\cdot y_k(i)x_k(i)^*|)}{I_0(|\bar{w}_{m,k}|)\exp(\mathsf{SNR}\cdot|x_k(i)|^2)}, \tag{19}$$

$$\hat{x}_{m,k}(i)=\arg\max_{x_k(i)\in\mathcal{X}}\rho_{m,k}(x_k(i)), \tag{20}$$

$$w_{m,k}=\bar{w}_{m,k}+2\cdot\mathsf{SNR}\cdot\mathbf{y}_k\hat{\mathbf{x}}_{m,k}^H, \tag{21}$$

$$\alpha_{m,k}=A\cdot\prod_i\rho_{m,k}(\hat{x}_{m,k}(i)), \tag{22}$$

where A is such that $\sum_{m=1}^M\alpha_{m,k}=1$.

References

[1] W. Shieh and Y. Tang, "Ultrahigh-speed signal transmission over nonlinear and dispersive fiber optic channel: the multicarrier advantage," *IEEE Photonics Journal*, vol. 2, no. 3, pp. 276–283, June 2010.

[2] L. B. Du and A. J. Lowery, "Optimizing the subcarrier granularity of coherent optical communications systems," *Optics Express*, vol. 19, no. 9, pp. 8079–8084, Apr. 2011.

[3] P. Poggiolini, A. Carena, Y. Jiang, G. Bosco, and F. Forghieri, "On the ultimate potential of symbol-rate optimization for increasing system maximum reach," in *Proc. of European Conference on Optical Communications, ECOC*, Sep. 2015, pp. 1–3.

[4] ——, "Analytical results on system maximum reach increase through symbol rate optimization," in *Proc. of Optical Fiber Communications Conference, OFC*, Mar. 2015, p. Th.3.D.6.

[5] M. Qiu, Q. Zhuge, M. Chagnon, Y. Gao, X. Xu, M. Morsy-Osman, and D. V. Plant, "Digital subcarrier multiplexing for fiber nonlinearity mitigation in coherent optical communication systems," *Optics Express*, vol. 22, no. 15, pp. 18 770–18 777, Jul. 2014.

[6] P. Poggiolini, A. Nespola, J. Y, G. Bosco, L. Carena, A Bertignono, B. S. M, S. Abrate, and F. Forghieri, "Analytical and experimental results on system maximum reach increase through symbol rate optimization," *IEEE Journal of Lightwave Technology*, vol. 34, no. 8, pp. 1872–1885, Apr. 2016.

[7] R. Dar and P. J. Winzer, "Nonlinear interference mitigation: Methods and potential gain," *IEEE Journal of Lightwave Technology*, vol. PP, no. 99, p. DOI:10.1109/JLT.2016.2646752, Jan. 2017.

[8] F. P. Guiomar, A. Carena, G. Bosco, L. Bertignono, A. Nespola, and P. Poggiolini, "Nonlinear mitigation on subcarrier-multiplexed PM-16QAM optical systems," *Optics Express*, vol. 25, no. 4, pp. 4298–4311, Feb. 2017.

[9] D. Marsella, M. Secondini, E. Agrell, and E. Forestieri, "A simple strategy for mitigating xpm in nonlinear wdm optical systems," in *Proc. of Optical Fiber Communications Conference, OFC*, Mar. 2015, p. Th.4.D.3.

[10] F. Buchali, W. Idler, K. Schuh, L. Schmalen, T. A. Eriksson, G. Böcherer, P. Schulte, and F. Steiner, "Study of electrical subband multiplexing at 54 GHz modulation bandwidth for 16QAM and probabilistically shaped 64QAM," in *Proc. of European Conference on Optical Communications, ECOC*, Sep. 2016, p. M.1.D.3.

[11] C. A, J. Renaudier, R. Rios-Müller, P. Tran, and G. Charlet, "Experimental analysis on non linear tolerance dependency of mulitcarrier modulations versus bandwidth efficiency," in *Proc. of European Conference on Optical Communications, ECOC*, Sep. 2015, p. Th.2.6.6.

[12] C. A, J. Renaudier, P. Tran, and G. Charlet, "Experimental analysis of non linear tolerance dependency of multicarrier modulations versus number of WDM channels," in *Proc. of Optical Fiber Communications Conference, OFC*, Mar. 2016, p. Tue.3.A.6.

[13] E. P. da Silva and D. Zibar, "Widely linear blind adaptive equalization for transmitter IQ-imbalance/skew compensation in multicarrier systems," in *Proc. of European Conference on Optical Communications, ECOC*, Sep. 2016, p. M.1.B.5.

[14] S. M. Bilal, C. Fludger, and G. Bosco, "Carrier phase estimation in multi-subcarrier coherent optical systems," *IEEE Photonics Technology Letters*, vol. 28, no. 19, pp. 2090–2093, Oct. 2016.

[15] M. Qiu, Q. Zhuge, M. Chagnon, F. Zhang, and D. V. Plant, "Laser phase noise effects and joint carrier phase recovery in coherent optical transmissions with digital subcarrier multiplexing," *IEEE Photonics Journal*, vol. 9, no. 1, p. 7901013, Feb. 2017.

[16] M. Pajovic, D. S. Millar, T. Akino-Koike, R. Maher, D. Lavery, A. Alvarado, M. Paskov, K. Kojima, K. Parsons, B. C. Thomsen, S. J. Savory, and P. Bayvel, "Experimental demonstration of multi-pilot aided carrier phase estimation for DP-64QAM and DP-256QAM," in *Proc. of European Conference on Optical Communications, ECOC*, Sep. 2015, p. Mo.4.3.3.

[17] D. S. Millar, R. Maher, D. Lavery, T. Koike-Akino, M. Pajovic, A. Alvarado, M. Paskov, K. Kojima, K. Parsons, B. C. Thomsen, S. J. Savory, and P. Bayvel, "Design of a 1 Tb/s superchannel coherent receiver," *IEEE Journal of Lightwave Technology*, vol. 34, no. 6, pp. 1453–1463, Mar. 2016.

[18] M. P. Yankov, L. Barletta, and D. Zibar, "Low-complexity joint sub-carrier phase noise compensation for digital multi-carrier systems," in *accepted, Proc. of European Conference on Optical Communications, ECOC*, Sep. 2017.

[19] L. Barletta, M. Magarini, and A. Spalvieri, "The information rate transferred through the discrete-time Wiener's phase noise channel," *IEEE Journal of Lightwave Technology*, vol. 30, no. 10, pp. 1480–1486, May 2012.

[20] M. P. Yankov, T. Fehenberger, L. Barletta, and N. Hanik, "Low-complexity tracking of laser and nonlinear phase noise in WDM optical fiber systems," *IEEE Journal of Lightwave Technology*, vol. 33, no. 23, pp. 4975–4984, Dec. 2015.

[21] M. P. Yankov, F. Da Ros, E. P. da Silva, S. Forchhammer, K. J. Larsen, L. K. Oxenløwe, M. Galili, and D. Zibar, "Constellation shaping for WDM systems using 256QAM/1024QAM with probabilistic optimization," *IEEE Journal of Lightwave Technology*, vol. 34, no. 22, pp. 5146–5156, Nov. 2016.

[22] D. M. Arnold, H. A. Loeliger, P. A. Vontobel, A. Kavčić, and W. Zeng, "Simulation-based computation of information rates for channels with memory," *IEEE Transactions on Information Theory*, vol. 52, no. 8, pp. 3498–3508, Aug. 2006.

[23] A. Barbieri and G. Colavolpe, "Soft-output decoding of rotationally invariant codes over channels with phase noise," *IEEE Transactions on Communications*, vol. 55, no. 11, pp. 2125–2133, Nov. 2007.

[24] G. Colavolpe, A. Barbieri, and G. Caire, "Algorithms for iterative decoding in the presence of strong phase noise," *IEEE Journal on Selected Areas in Communications*, vol. 23, no. 9, pp. 1748–1757, Sep. 2005.

[25] M. P. Yankov, F. Da Ros, E. P. da Silva, T. Fehenberger, L. Barletta, D. Zibar, L. K. Oxenløwe, M. Galili, and S. Forchhammer, "Nonlinear phase noise compensation in experimental WDM systems with 256QAM," *IEEE Journal of Lightwave Technology*, vol. PP, no. 99, p. DOI:10.1109/JLT.2016.2644860, Dec. 2016.

[26] ——, "Experimental study of nonlinear phase noise and its impact on WDM Systems with DP-256QAM," in *Proc. of European Conference on Optical Communications, ECOC*, Sep. 2016, p. W.1.D.1.

[27] S. T. Le, A. D. Haigh, P A an Ellis, and S. Turitsyn, "Blind phase noise estimation for CO-OFDM transmissions," *IEEE Journal of Lightwave Technology*, vol. 34, no. 2, pp. 745–753, Jan. 2016.

[28] G. Durisi, A. Tarable, C. Camarda, R. Devassy, and G. Montorsi, "Capacity bounds for MIMO microwave backhaul links affected by phase noise," *IEEE Transactions on Communications*, vol. 62, no. 3, pp. 920–929, Mar. 2014.